



HAL
open science

Experimental Investigation of Mechanical Properties of Additively Manufactured Fibre-Reinforced Composite Structures for Robotic Applications

Arnav Bisoi, Mertol Tüfekci, Vehbi Öztekin, Enora Denimal Goy, Loïc Salles

► To cite this version:

Arnav Bisoi, Mertol Tüfekci, Vehbi Öztekin, Enora Denimal Goy, Loïc Salles. Experimental Investigation of Mechanical Properties of Additively Manufactured Fibre-Reinforced Composite Structures for Robotic Applications. *Applied Composite Materials*, 2023, pp.1-26. 10.1007/s10443-023-10179-9 . hal-04336788

HAL Id: hal-04336788

<https://hal.science/hal-04336788>

Submitted on 8 Jan 2024

HAL is a multi-disciplinary open access archive for the deposit and dissemination of scientific research documents, whether they are published or not. The documents may come from teaching and research institutions in France or abroad, or from public or private research centers.

L'archive ouverte pluridisciplinaire **HAL**, est destinée au dépôt et à la diffusion de documents scientifiques de niveau recherche, publiés ou non, émanant des établissements d'enseignement et de recherche français ou étrangers, des laboratoires publics ou privés.



Distributed under a Creative Commons Attribution 4.0 International License



Experimental Investigation of Mechanical Properties of Additively Manufactured Fibre-Reinforced Composite Structures for Robotic Applications

Arnav Bisoi¹ · Mertol Tüfekci¹ · Vehbi Öztekin² · Enora Denimal Goy^{1,3} · Loïc Salles^{1,4}

Received: 24 August 2023 / Accepted: 6 November 2023
© The Author(s) 2023

Abstract

This study explores the variation in mechanical properties of additively manufactured composite structures for robotic applications with different infill densities and layer heights using fused deposition modelling (FDM). Glass fibre-reinforced polyamide (GFRP), and carbon fibre-reinforced polyamide (CFRP) filaments are used, and the specimens are printed with 20%, 40%, 60% and 100% infill density lattice structures for tensile and three-point bending tests. These printed samples are examined in the microscope to gain more understanding of the microstructure of the printed composites. To characterise the mechanical properties, a set of tensile and three-point bend tests are conducted on the manufactured composite samples. Test results indicate the variations in tensile strength and Young's modulus of specimens based on the printing parameters and reveal the tensile and bending behaviour of those printed composite structures against varying infill ratios and reinforcing fibres. The experimental findings are also compared to analytical and empirical modelling approaches. Finally, based on the results, the applications of the additively manufactured structure to the robotic components are presented.

Keywords Additive manufacturing · Composites · Mechanical characterisation · Mechanical testing · Robotic applications

✉ Mertol Tüfekci
m.tufekci17@imperial.ac.uk

¹ Department of Mechanical Engineering, Imperial College London, Exhibition Road, London SW7 2AZ, United Kingdom

² Faculty of Mechanical Engineering, Istanbul Technical University, İnönü Cd. No 65 Gümüşsuyu, İstanbul 34437, Turkey

³ Université Gustave Eiffel, COSYS-SII, I4S, 35042 Rennes, Inria, France

⁴ Department of Aerospace and Mechanical Engineering, Mechanical Aspects of Turbomachinery and Aerospace Propulsion, University of Liège, 4000 Liège, Belgium

1 Introduction

Additive Manufacturing (AM) has been extensively used in the industry for prototyping, mostly using polymeric materials [1–3]. However, AM is rarely used to manufacture safety-critical components since it is difficult to predict the mechanical properties of the printed components. ASTM F2792 states seven categories of AM techniques, namely: vat photo-polymerisation, material jetting, binder jetting, material extrusion, powder bed fusion, sheet lamination and directed energy deposition [4]. The selection of an appropriate AM technique depends on factors such as the minimum strength requirement, budget/setup cost, quantity and dimensions of the components [5, 6].

Fused deposition modelling (FDM) is based on feeding a spool of thermoplastic material to a liquefier which deposits the molten material onto the printing bed along a predetermined trajectory [7]. Slicing software is used to generate the trajectory and set other printing parameters which dominantly influence the mechanics of the printed structures. The printer's bed height decreases on completion of each layer, and consecutive layers are extruded on top of the previous layer. Moreover, the liquefaction process is regulated by controlling the nozzle and heatsink temperatures. Cooling fans blow cold air on the heatsinks to prevent heat creep, which can lead to blockages in the extruder. However, the cooling process for the component being printed is largely uncontrolled. Slicing software allows users to modify the printing parameters according to requirements such as printing time, cost, weight and surface finish, and these parameters have an impact, which is given in Table 1, on the strength of the printed component.

The printing time is prioritised when multiple copies of the same component must be printed. An increase in infill percentage/shell thickness or a decrease in layer height leads to an increase in printing time. The surface finish is prioritised for components that can be seen and touched by the user. The surface finish improves with a decrease in the layer height. Overall, the printing parameters must be optimised for individual prints and materials [8–12].

Slicing software generally provides 3–4 options for infill patterns, including but not limited to concentric, honeycomb and rectilinear. The choice of infill pattern affects the weight, strength, stiffness and printing time of the component [13]. The study by Khan et al. found that 100% infill density specimens with the rectilinear pattern had a higher tensile strength as compared to their honeycomb counterparts [10]. Additionally, the rectilinear specimens were found to be 6.8% lighter as well. The study by Fernandez-Vincente

Table 1 Printing parameters and their effect on tensile strength

Parameter	Effect on Tensile Strength	Reason
Layer Height	Tensile strength first decreases, then increases with an increase in layer height Increase in infill density leads to an increase in tensile strength	Improved layer adhesion [14] Minimisation of distortion [15] Reduction in the number of voids [16] Reduction in volume of air gaps [16, 17]
Shell Thickness	Increase in the number of shells/shell thickness leads to an increase in tensile strength	The shell acts as a solid layer at the periphery of the print [18, 19]
Infill Density	Higher infill density, higher stiffness and strength.	The load distribution is inefficient, with low-stress areas indicating excess material use [20–23].

et al. found that honeycomb specimens have a higher tensile strength as compared to their rectilinear counterparts for low infill densities, but the results are reversed for the 100% infill density [17]. In honeycomb specimens, all layers are printed along the same trajectory; however, in rectilinear specimens, the orientation of consecutive layers alternates by 90°. Due to this rotation, the extruded lines must bridge the gaps in the previous layer, which creates voids. These voids decrease in size with an increase in infill density and are minimised at 100% infill density [24, 25]. Besides, for the parts, that are designed to be printed along the z-axis, a compressive load would improve layer adhesion and close small voids, thereby improving their mechanical performance.

There are four major sources of anisotropy in addition to the laminar nature, which significantly affects the stiffness and strength of FDM prints: variation in printing parameters and environmental conditions, anisotropy in the filament itself and thermal gradients generated by non-uniform cooling and of course, the geometry of the infill pattern [26–31]. Starting with factors related to the environment, for instance, fluctuations in the nozzle temperature can lead to varying filament liquefaction that causes inhomogeneous layer adhesion properties and thus gaps can form in between layers [32]. Similarly, the moisture absorbed by the filament or the debris entering into the printing environment can cause poor layer adhesion and consequently warping of the printed structure. Moreover, filament diameter may vary during extrusion due to partial/temporary blockages in the nozzle. This causes non-uniform mass flow which is a common and hard-to-control phenomenon. Also, using reinforcement in the filament has an impact on the anisotropy of the printed structure. As in conventional composite applications, reinforcement phases are added to the material to increase the strength and stiffness as well as for toughening reasons. Long/continuous fibre-reinforced filaments display anisotropic nature [33–37], as well as whisker-reinforced [38] filaments. The use of natural fibres is also becoming more common to achieve more sustainability [2, 39]. Even though, short-fibre and/or particle-reinforced filaments show quasi-isotropic behaviour due to random positioning and orientation [40–45], filament liquification changes fibre orientation and distribution (density) across the print. To get an orientation extra caution is required as well as additional methods [46, 47].

In the current landscape of additive manufacturing of fibre-reinforced composites, various studies have focused on different aspects of the technology. For instance, Naima Khalid et al. [48] reviewed the mechanical properties and interlayer bonding in continuous carbon fibre-reinforced polyamide-6 composites. Similarly, Abderrafai et al. investigated the mechanical properties of short carbon fibre-reinforced Polyamide 12, highlighting the effects of environmental temperature and infill patterns [49]. Al Rashid et al. examined how infill patterns and densities influence the mechanical performance of carbon fibre-reinforced Polyamide-6 [50]. Palanikumar et al. reviewed additive manufacturing techniques for fibre-reinforced composite materials [51]. While Jansson and Pejryd characterised carbon fibre-reinforced polyamide manufactured by selective laser sintering [52]. Lastly, Al Abadi et al. developed an analytical model to predict the elastic properties of 3D-printed fibre-reinforced polymers [44].

There are several studies focused on optimising the printing parameters and trajectory in a bid to reduce the anisotropic behaviour [5, 30, 53]. The printing path, also known as the Hybrid Deposition Path (HDP) can be optimised to increase the directional strength while minimising overall volume [54]. Printing parameters, including the layer height and infill density, can also be tuned to minimise the volume of the print without compromising the strength [55]. However, if isotropic properties are assumed, the implementation of any modelling and/or optimisation work becomes simpler as it eliminates the need to account for material complexities like direction-dependent behaviour.

FDM printers do not regulate the temperature of the component being printed, and as a result, it undergoes non-uniform cooling. This leads to large thermal gradients and residual stresses [56]. Once the print is released from the printing bed, these residual stresses can cause warping [57, 58], and adversely affect the dimensions [59] and shape [60] of the print. Studies have shown that mechanical properties, including yield strength [61] and strain at failure [62], are also affected by thermal gradients.

It is also important to stress that, the AM process brings its own risks of creating a hazardous environment, and therefore, the parameters, including printing and ambient temperature as well as ventilation, must be arranged carefully. The AM process should not only be designed and conducted based on the mechanical performance of the outcoming product [63].

This study deals with the investigation of the effects of the layer height and reinforcing phase, which is the fibres, on the mechanical properties of additively manufactured fibre-reinforced composite structures for robotic applications. For this purpose, sample composite structures are prepared using AM. The process of FDM is selected for this project due to its accessible cost, wide range of materials and relatively quick production time [58, 64]. To execute the manufacturing for the study, the Raise3D printer is used, which can print basic thermoplastics and fibre-reinforced filaments since its nozzle temperature can reach 300°C. Polyetheretherketone (PEEK) and Polyetherimide (ULTEM) are the best materials for FDM printing when considering strength and durability [65]. However, both PEEK and ULTEM require nozzle temperatures close to 500 °C due to their high melting point. Since the Raise3D printer can only reach nozzle temperatures of 300 °C, fibre-reinforced polyamides are the best choice. Polymaker's (20%) carbon fibre-reinforced polyamide (CFRP) and XSTRAND's (30%) glass fibre-reinforced polyamide (GFRP) filaments are selected for this project due to their high strength and stiffness. These structures are planned to consist recilinear infill pattern since the printing of this pattern is relatively easy and excels in all the aforementioned factors. Besides, there is a relatively limited number of studies focusing on that pattern. Samples with different infill ratios, as well as layer heights, are manufactured to explore the effects of those parameters on the mechanical properties. The manufactured samples are put through a set of experimental procedures which includes microscopic visualisation of the microstructure and tensile and three-point bend tests. The test results are also compared to theoretical models, including Voigt and Reuss, self-consistent, and Halpin-Tsai approaches to discuss the effects of the reinforcements and AM process. Finally, the robotic application of the additively manufactured structures that are tested and discussed are presented in detail. AM is chosen for building robot parts for two main reasons. First, AM makes it possible to create complex shapes that are worked out using topology optimisation (TO) [66]. Second, AM helps to lighten the weight by adjusting both the outer shape through TO and the material used inside the part, through reduction of the amount of the material used for the infill structure. In this context, the tested structures have applications in robotics. These structures are designed with the help of finite element analysis (FEA) and topology optimisation, and can be made efficiently using AM. This offers the benefits mentioned earlier. This study offers a fresh perspective on the relationship between printing parameters and the mechanical characteristics of fibre-reinforced composites. It uniquely combines microscopic analysis with tensile and three-point bend tests to offer a comprehensive characterisation of material behaviour. Furthermore, this work extends beyond mere material testing by incorporating analytical and empirical modelling approaches for structural optimisation. This includes the use of topology optimisation techniques to identify optimal structures, thereby contributing to material efficiency and reducing the overall weight of the robotic components.

2 3D Printing of Samples

Raise3D printer is utilised to manufacture the samples. GFRP and CFRP materials are selected to produce the specimens with the FDM method. The specimens are produced with two different layer heights, four different infill densities and two different materials, all summarised in Table 2 [67–69].

The data provided by the manufacturer is based on only 100% infill density test specimens. The experiments are conducted to find the effective mechanical properties of FDM printed specimens. The experimental results are also used to quantify the effect of infill density and layer height on the mechanical properties.

ASTM D638 and ASTM D790 were selected for the tensile test and three-point bend test specimens, respectively. ASTM D638 presents the standard test method for tensile test properties of plastics [70], whereas ASTM D790 presents the standard test method for flexural properties of unreinforced and reinforced plastics and electrical insulating material [68]. These standards are not dedicated to FDM printed specimens; however, they have been used in similar studies [69]. The sample dimensions based on these mentioned standards are shown in Fig. 1.

Multiple infill densities were selected to facilitate the prediction of intermediate properties using interpolation. Layer heights of 0.05 mm and 0.2 mm were selected so that their strength and printing time could be compared. The tensile strength is known to be in correlation to the number of shells; three shells were selected since that is a good compromise between strength and printing time. Shells are necessary to preserve the structural integrity of the samples preventing premature buckling and/or failure of the infill structure. As they are kept constant throughout this research. Thus, it is ensured that the shells do not affect the variations of mechanical properties observed against changing parameters.

Table 2 Materials and printing parameters for test specimens

Materials	Specimen Type	Layer Height	Infill Density
Polymaker PA6-CF and XSTRAND GF-PA6	Tensile Test	0.05 mm	20%
	Tensile Test	0.05 mm	40%
	Tensile Test	0.05 mm	60%
	Tensile Test	0.05 mm	100%
	Three-Point Bend Test	0.05 mm	100%
Polymaker PA6-CF and XSTRAND GF-PA6	Tensile Test	0.2 mm	20%
	Tensile Test	0.2 mm	40%
	Tensile Test	0.2 mm	60%
	Tensile Test	0.2 mm	100%
	Three-Point Bend Test	0.2 mm	100%

Each specimen has three layers of shells

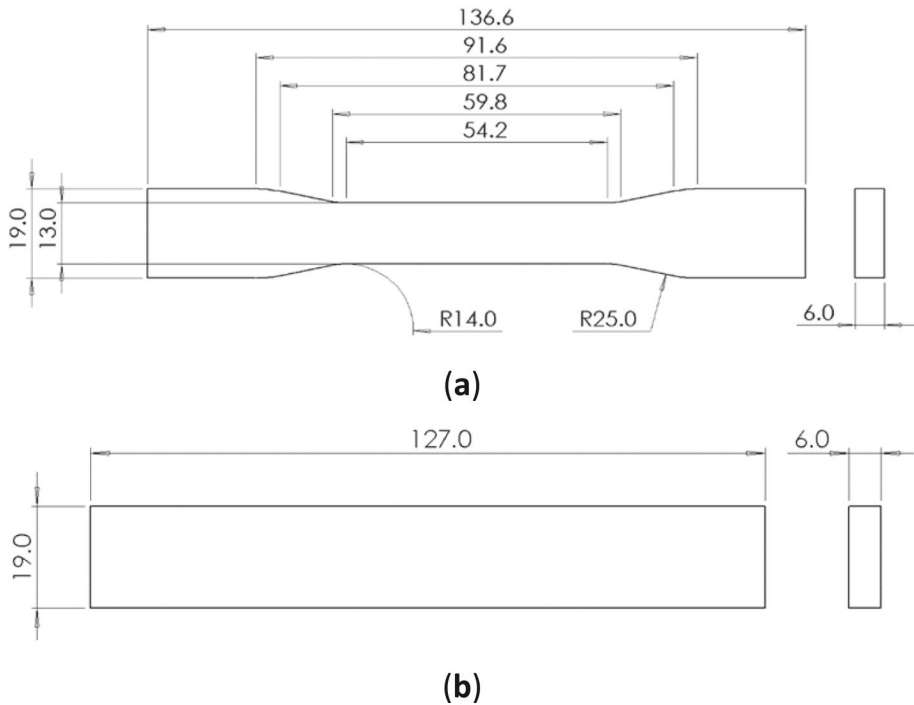


Fig. 1 Schematic view of samples printed for experiments. **a** Tensile test specimens; **b** three-point bend test specimens

3 Experimental Study

The experimental study consisted of two main parts, visual examinations of the microstructure through a microscope and mechanical tests. Tensile and three-point bend tests are conducted to obtain the deformation characteristics of the different materials. Visual examinations are done to visualise the surface of the material.

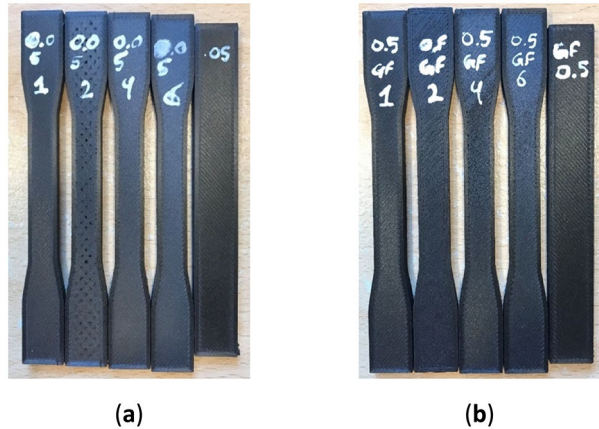
3.1 Visual Examinations

Specimens are examined with a Nikon SMZ800 stereo microscope under various magnifications. The examinations are conducted to gain more understanding of the microstructure and surface properties of the printed samples.

3.2 Mechanical Tests

Two sets of carbon fibre (CF) and glass fibre (GF) tensile and three-point bend test specimens are shown in Fig. 2. All the specimens have a layer height of 0.05 mm, and the numbers 2, 4, 6 and 1 indicate 20%, 40%, 60% and 100% infill densities. The CF test specimens are easily distinguishable due to their smooth surface finish. To achieve reliable and repeatable results, experiments are conducted for each parameter until at least

Fig. 2 Test specimens; **a** GF test specimens, **b** CF test specimens



three sets of consistent data are acquired and the averaged values are presented as the results. The specimen groups based on material and printing layer height are presented in Table 2.

3D prints are porous in nature, and fibre-reinforced filaments are hygroscopic; this makes the specimens susceptible to moisture absorption. Since moisture can alter the mechanical properties, all specimens are annealed at 70 °C for 2 hours. Moisture absorption can also cause warping, which can change the overall dimensions. Before the experiments, all specimens are measured with a vernier calliper, and their dimensions are recorded. Metal tabs are fixed to the ends of the tensile test specimens to improve grip in the clamp. Lastly, both tests are conducted with a constant strain rate of 0.5% per minute and the displacements are measured with the attached extensometer, which is a Shimadzu DVE-201 noncontact video extensometer. Figure 2 shows the specimens, and Fig. 3 images of the test setups whilst the experimentation is being performed.

While it is generally expected that an increase in infill density would result in a more durable structure with increased strength and elastic modulus, it remains essential to quantify these changes, especially in the context of fibre-reinforced composites for robotic applications. The investigation into varying infill densities provides specific data that can be used for optimising the mechanical performance and material efficiency of the robotic components. Furthermore, the study aims to explore how infill density interacts with other variables, such as types of reinforcing fibres and layer heights, to offer a comprehensive understanding of the material's mechanical behaviour.

4 Modelling of the Fibre-Reinforced Composites

Understanding the mechanical behaviour of fibre-reinforced composites requires understanding various theoretical frameworks. These models provide a reasonable estimate of key mechanical properties, such as Young's modulus that can be compared against experimental data.

In the analysis, the mechanical properties of the individual phases, the matrix and the reinforcing fibres are taken from the literature as their mechanical properties are not provided by the manufacturer and it is practically not possible to measure them. Specifically, the elastic

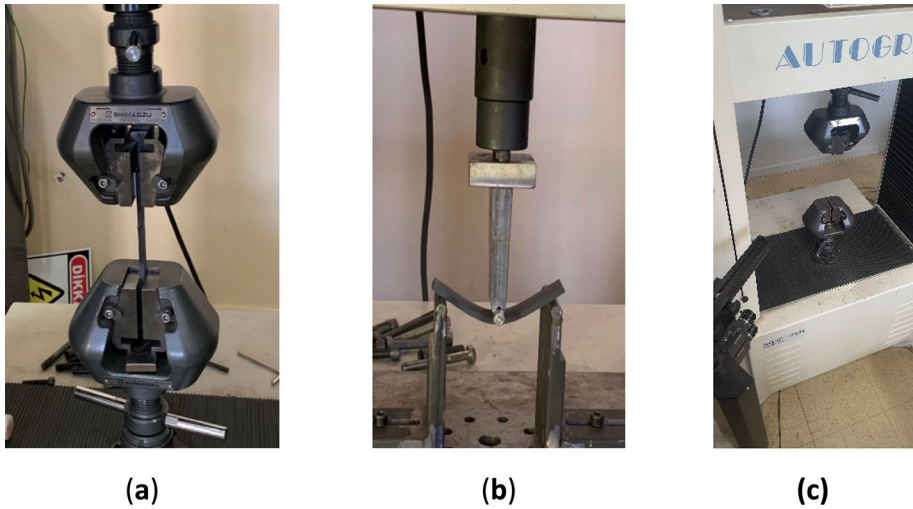


Fig. 3 Test specimens during tests; **a** Tensile test **b** three-point bend test **c** Tensile test setup with the extensometer

modulus of carbon fibre is $E_{\text{carbon fibre}} = 200$ GPa, that of glass fibre is $E_{\text{glass fibre}} = 40$ GPa, and for polyamide, it is $E_{\text{polyamide}} = 0.2$ GPa [48, 64, 71–74]. The volume fractions of the fibres in the composite materials are provided by the manufacturer. For the Polymermaker's CFRP, the volume fraction V_{CF} is 0.2, and for XSTRAND's GFRP, the volume fraction V_{GF} is 0.3. These parameters are critical for understanding the mechanical behaviour of the composites under various loading conditions.

4.1 Voigt and Reuss Approximations

The Voigt and Reuss models are refined approximations. The Voigt model, also known as the parallel model, assumes that the strain is constant throughout the composite, thus providing an upper bound on the composite's stiffness which is represented as E_{Voigt} . Conversely, the Reuss model assumes that the stress is constant throughout the composite, thus serving as a lower bound denoted as E_{Reuss} .

$$E_{\text{Voigt}} = E_f V_f + E_m (1 - V_f) \quad (1)$$

$$E_{\text{Reuss}} = \frac{1}{\frac{V_f}{E_f} + \frac{1-V_f}{E_m}} \quad (2)$$

Here, E_f and E_m denote the Young's moduli of the fibre and matrix, respectively, and V_f represents the volume fraction of the fibres.

4.2 Self-Consistent Scheme

The self-consistent Scheme extends beyond simplistic assumptions to cater to composites with more complex microstructures. The self-consistent scheme assumes that the

inclusions are embedded in an infinite matrix, making it particularly useful for randomly oriented fibres or particles since it accounts for the interactions between neighbouring inclusions. It employs an iterative method, beginning with an initial approximation for the effective modulus (E_{eff}), which is refined until a satisfactory convergence is achieved. The effective Young's modulus can be represented as:

$$E_{\text{eff}} = E_m \left(1 + \frac{3V_f(E_f/E_{\text{eff}} - 1)}{1 + V_f(E_f/E_{\text{eff}} - 1)} \right) \quad (3)$$

4.3 Halpin-Tsai Model

The Halpin-Tsai equations are semi-empirical models used to predict the elastic moduli of composite materials with randomly-oriented fibres. These equations introduce two empirical parameters, η_L and η_T , to fine-tune the effective longitudinal and transverse Young's moduli. The model accounts for the aspect ratio and orientation of the fibres, but it requires empirical calibration. Parameters η_L and η_T should ideally be obtained from experimental measurements, making the model a blend of theory and empiricism.

The effective longitudinal ($E_{\text{eff,long}}$) and transverse ($E_{\text{eff,trans}}$) moduli can be represented as:

$$E_{\text{eff,long}} = E_m \left(1 + \frac{\eta_L V_f (E_f/E_m - 1)}{1 - \eta_L V_f (E_f/E_m - 1)} \right) \quad (4)$$

$$E_{\text{eff,trans}} = E_m \left(1 + \frac{\eta_T V_f (E_f/E_m - 1)}{1 - \eta_T V_f (E_f/E_m - 1)} \right) \quad (5)$$

As explained, the Halpin-Tsai equations include additional material parameters, η_T and η_L , to capture the anisotropic nature of composite materials. In the Halpin-Tsai model, the values of η_L and η_T are selected as $\eta_L=3$ for the longitudinal behaviour and $\eta_T=1.5$ for the transverse behaviour when considering the Polymaker's CFRP. For XSTRAND's GFRP, $\eta_L=2.5$ and $\eta_T=1.0$ are utilised. These choices in η values are guided by the aspect ratios and the degree of fibre alignment in the composite material.

5 Application of the Additively Manufactured Structures to Robotics

This section focuses on the application of the additively manufactured structures, that are thoroughly examined and tested in the preceding sections, in robotics. Specifically, the spotlight is on the design of drivetrain skirts and support plates, which are important structural components, of the robot in the design process (see Fig. 4). Taking advantage of the findings from the material testing part of this research, improvements have been made in both exterior design, infill ratio and material selection for these components. FEA and TO, which aim to limit the stress and deflections whilst minimising the mass of the structure, are employed to achieve these design improvements, laying the groundwork and preparing the components for practical implementation. To check the final

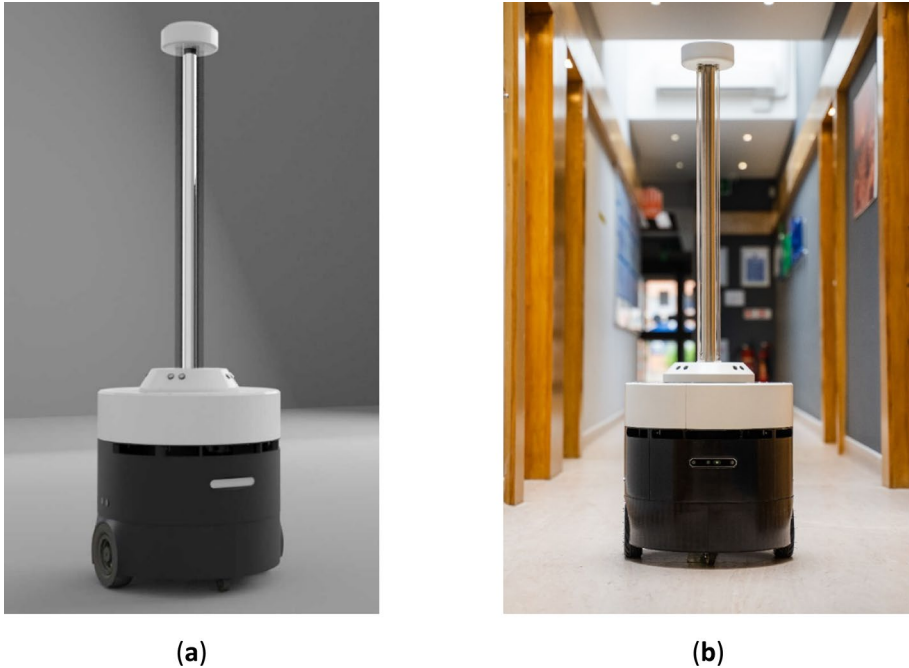


Fig. 4 The robot in development **a** CAD render **b** Photo of the assembled robot prototype

design that considers manufacturability and other operational factors, static FEA for each component is performed.

5.1 Drivetrain Skirts

The drivetrain module is designed first since it is required for testing the electronics. Once the circular cross-section is decided, the drivetrain components are fit within the smallest possible area, which is a circle of diameter 430 mm. The build area of the Raise3D printer is only 300 mm by 300 mm, which meant the skirts could not be printed as one single part and has to be divided into four sections.

The skirts are designed to be sandwiched between the Aluminium plates creating a tortoiseshell capable of bearing a 100 kgf load. The wall thickness of the first design is 11 mm and the flanges on the top and bottom are 7 mm wide. The circular cut-out acted as a wheel arch for the driven wheels which are attached to the sides of the robot. The flange sticking out from the side of the skirt coupled with complimentary flanges on the adjacent skirt such that both skirts could be secured with one bolt.

A load of 45 kg (441.5 N) is applied on the top flange of the skirt, and this value included a safety factor which accounted for any discrepancies in the manufacturers' data. An 'Encastre' boundary condition is applied on the bottom flange of the skirt to model the support from the bottom plate. Since the design has sharp corners and complex curves, a free-form tetrahedron mesh is used. The initial design, boundary conditions and the loading are visualised in Fig. 5.

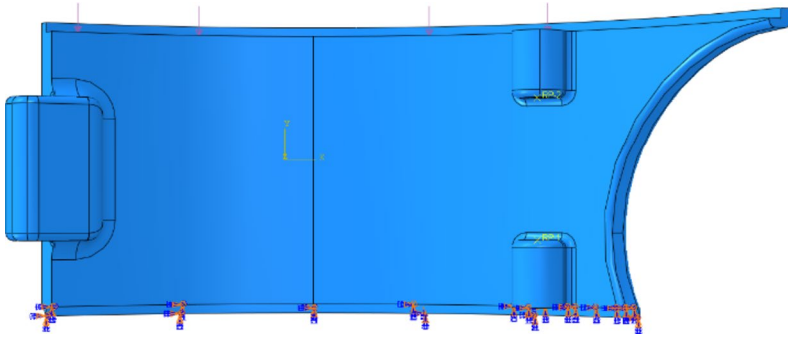


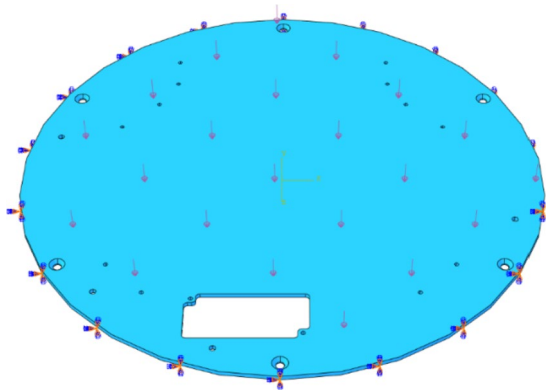
Fig. 5 Applied load and boundary conditions on the initial design of the drivetrain skirts

5.2 Support Plates

All plates are required to support M4 and M5 threads, standards dictate a minimum thickness of 5mm to support these threads in a medium strength metal. High strength 6082-grade Aluminium is selected as this allowed the use of 4mm plates without compromising the threads. The drivetrain module bottom plate is not suitable for material reduction since it is packed with components. Also, openings in the bottom plate would make the robot susceptible to debris ingress when travelling over rough terrain. Similarly, material could not be removed from the UV module plates since that would expose high voltage components. Only the drivetrain module top plate is suitable for material reduction and a TO is conducted to identify the most suitable regions.

This study models the worst-case scenario wherein a load of 50 kgf (490N) is applied over the entire surface and the plate is fixed at its circumference with an ‘Encastre’ boundary condition. The load, boundary conditions applied on the initial design of the plate are shown in Fig. 6.

Fig. 6 Applied load and boundary conditions on the initial design of the support plates



6 Results and Discussions

6.1 Visual Examinations

The images of the surfaces of the test specimens acquired through the microscopy are presented in Figs. 7, and 8 shows the images of the outer shells of the printed samples. The layered and porous nature of the samples is observed clearly. Moreover, the images also show that the surface roughness of the samples is relatively high. This is due to the fact that 3D-printed parts are typically made up of many individual layers, which can create a rough surface. The surface roughness can affect the mechanical properties of the samples, so it is important to consider this when designing and testing 3D-printed parts. However, the surfaces show no major inconsistency nor any significant flaw. Therefore, it is possible to assume that the printing process is completed successfully to achieve the necessary consistency, which would allow the investigation of the effects of the printing parameters and the filament materials used on the mechanics of the samples.

6.2 Mechanical Tests

The deformation characteristics of all specimens are indicated in Fig. 9. The graphs show an increase in the ultimate tensile strength (UTS) with an increase in infill density due to the increase in material volume. The 100% infill lines (red) show almost a parabolic increase, indicating non-linear behaviour. Non-linear behaviour is caused by large displacements and the presence of defects in the printed specimens. The sharp and short dip right

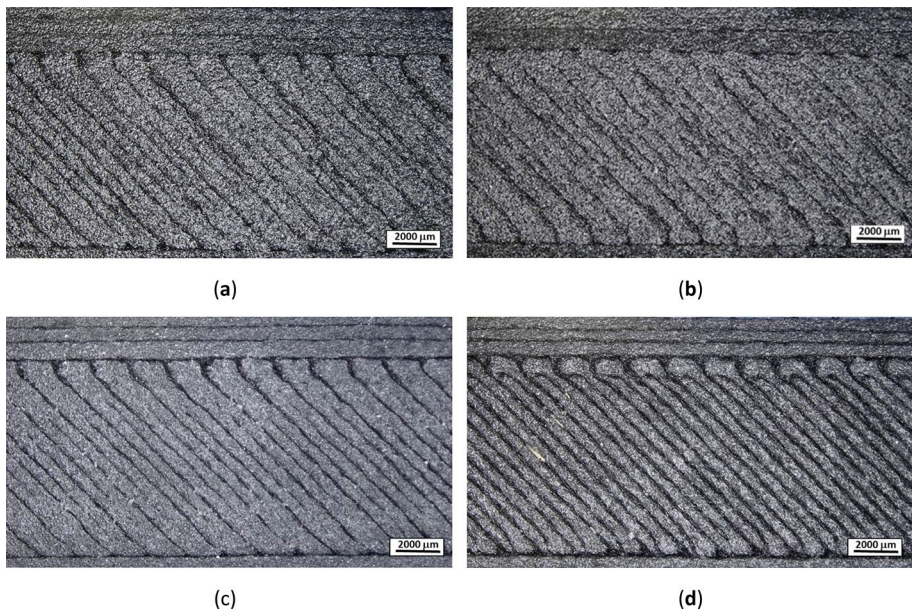


Fig. 7 Images of the infill structure of 100% infill density tensile specimens. **a** CF with 0.2 mm layer height, **b** CF with 0.05 mm layer height, **c** GF with 0.2 mm layer height and **d** GF with 0.05 mm layer height

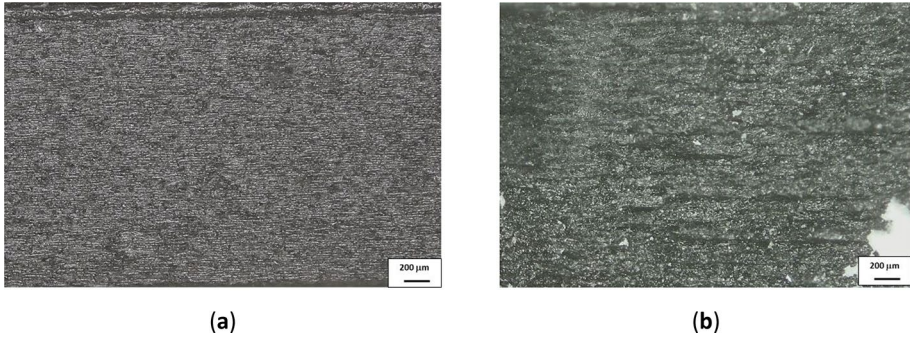


Fig. 8 Images of surfaces of the outer shells of CF samples with **a** 0.2 mm and **b** 0.05 mm layer heights

after UTS indicates brittle behaviour, which is consistent with fibre-reinforced composites. The sharp dip can also be caused by cracks prevalent in FDM prints due to their laminar structure.

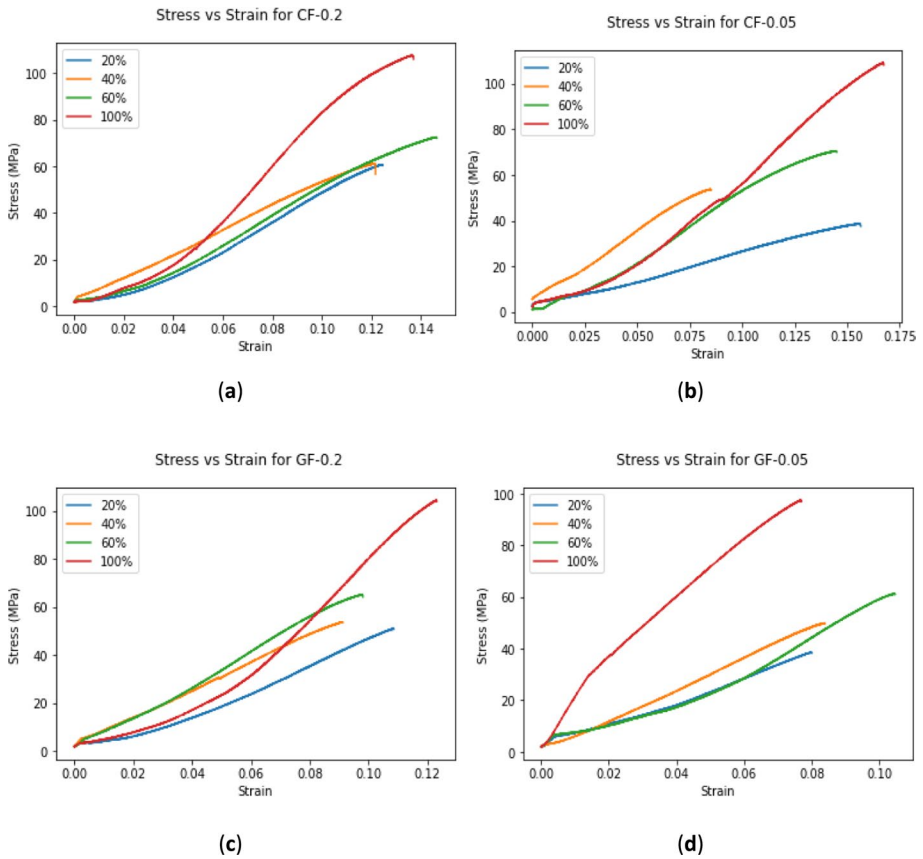


Fig. 9 Stress vs Strain graphs for; **a** CF-0.2mm layer height, **b** CF-0.05mm layer height, **c** GF-0.2mm layer height, **d** GF- 0.05mm layer height. All values are presented in MPa

The 0.2 mm layer height specimens for both materials show a higher UTS as compared to their 0.05 mm layer height counterparts. Additionally, the UTS for the GF specimens is higher than the UTS for the CF specimens for both layer heights. This suggests the use of GF over CF if the tensile strength is crucial for the component. This difference in performance between glass and CF is in line with the data provided by XSTRAND and Polymaker.

The results obtained from tensile tests are indicated in Fig. 10 regarding the ultimate tensile strength (a), and Young Modulus (b) for all the parameters. UTS values have almost the same increasing trend for both materials. There are no significant differences between 20% and 40% infill densities, except GF 0.05. The difference between 20% and 40% infill density increases UTS for GF 0.05. Also, GF 0.05 have a more linear UTS increasing trend.

Moreover, all the materials have reached their peak UTS values at 100% infill densities, as expected. Also, the materials have the same trend in terms of UTS for 20%, 40% and 60% infill densities, but this trend does not hold for 100% infill densities. Some material flaws like interlayer shear, layer shift, moisture absorption and voids due to printing could be the reason for the difference.

The graph in Fig. 10b shows a monotonic increase in Young's modulus values with an increase in infill density. This can be attributed to an increase in material volume with an increase in infill density. Theoretically, the 0.2 mm layer height specimens should have a higher Young's modulus compared to their 0.05 mm counterparts. This trend is followed for all infill densities except for 20% in CF and 100% in GF, where the results are reversed. This is likely caused by the defects mentioned above, such as layer shifts, moisture absorption and voids in the specimen as they are known to reduce stiffness [14, 75–79]. The results are also presented in Tables 3 and 4.

The stress-strain curves of acquired from the three-point bend tests are presented in Fig. 11. Also, the flexural strength and flexural modulus for each set of material and layer height are visualised and compared in Fig. 12 and Table 5. Both flexural strength and modulus are significantly higher for 0.05 mm layer height for CF and GF. Compared to the CF specimens with 0.05 mm layer height, GF specimens show improved stiffness and strength for the same layer height. On the other hand, CF specimens display better performance for 0.2 mm layer height compared to the GF specimens with the same layer height, but the difference is not as noticeable.

The characterisation analysis of the effects of infill densities and layer heights on the mechanical properties of additively manufactured GFRP and CFRP composite structures indicate clear patterns in surface/microstructural properties, strength, and stiffness, mostly aligning with theoretical expectations. The microscopy visuals reveal the surface roughness and consistency of the printed samples, whilst the mechanical tests show the influence of infill density and layer height on the tensile and flexural properties. It is shown that the inherent complexities and non-linearities in 3D-printed composite structures are strongly linked to the material's structural irregularities/inhomogeneities and defects. Inconsistencies observed in some trends are related to these internal/microstructural irregularities in the printing process, emphasising the importance of quality control and precise parameter selection and optimisation. The preference for GF over CF to achieve improved strength, the role of infill density and the significant variations of the effective mechanical properties between different layer heights collectively contribute to a more comprehensive understanding of how to fine-tune the printing parameters to attain the desired mechanical properties. These findings highlight the complexity of 3D printing process, particularly with composite materials and stress the potential for further exploration, including statistical analyses, material flaw investigation, and

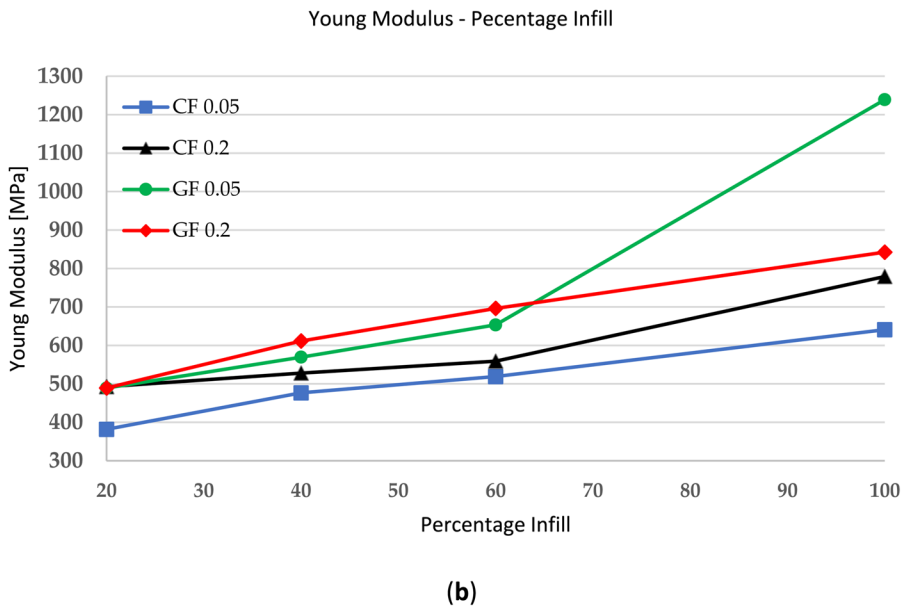
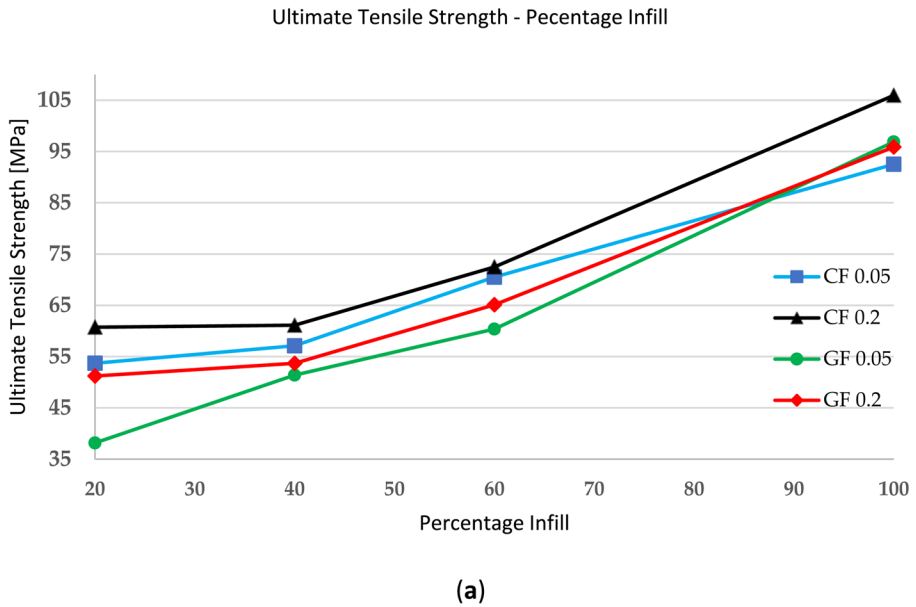


Fig. 10 Comparison between UTS (a) and Young’s modulus (b) due to infill percentage. All values are presented in MPa

exploration of various polymer-fibre combinations to develop better tailorable materials and structures, enhancing the understanding of how to design and produce parts that meet specific mechanical needs.

Table 3 Tensile strengths and Young's moduli for CF specimens

Experimental Results for CF	20% Infill Density	40% Infill Density	60% Infill Density	100% Infill Density
Tensile Strength (CF-0.2) [MPa]	62.4	54.5	72.5	105.9
Young's Modulus (CF-0.2) [MPa]	404.4	446.7	537	727.1
Tensile Strength (CF-0.05) [MPa]	39.1	55.4	70.5	92.5
Young's Modulus (CF-0.05) [MPa]	381.8	476.2	518.9	652.4

All values are presented in MPa

Table 4 Tensile strengths and Young's moduli for GF specimens

Experimental Results for GF	20% Infill Density	40% Infill Density	60% Infill Density	100% Infill Density
Tensile Strength (GF0-0.2) [MPa]	51.2	48.8	55.6	95.8
Young's Modulus (GF-0.2) [MPa]	515.4	616.5	673	842.5
Tensile Strength (GF0-0.05) [MPa]	38.2	51.4	60.4	96.8
Young's Modulus (GF-0.05) [MPa]	489.1	569.3	653.3	1238.8

All values are presented in MPa

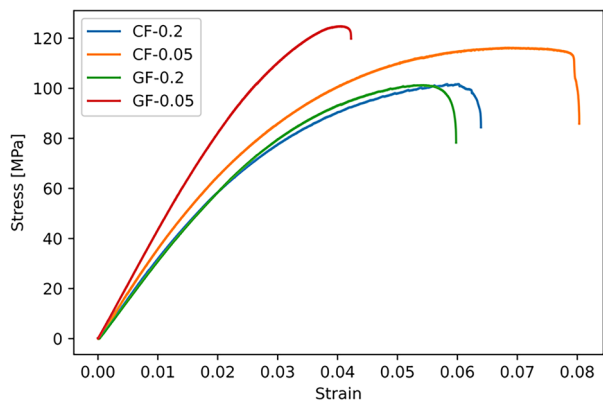
6.3 Modelling of the Fibre-Reinforced Composites

In analysing the effective moduli of carbon and glass fibre-reinforced polymers, multiple homogenisation techniques are employed. These include the Voigt and Reuss bounds, the self-consistent method, and the Halpin-Tsai model. These results and their comparisons against the experimental data is presented in Fig. 13 and Table 6.

For Voigt and Reuss methods, E_{Voigt} and E_{Reuss} represent upper and lower bounds, respectively, for the effective stiffness of the composite. In CFRP samples, these bounds are 40160 MPa and 249.9 MPa. For GFRP samples, the bounds are 12140 MPa and 285.1 MPa.

The self-consistent method provides an effective modulus for CFRP and GFRP, E_{eff} of 788.4 MPa and 763.5 MPa, respectively. Unlike the Voigt and Reuss bounds, this method

Fig. 11 Stress vs Strain graphs for the three-point bend samples. Stress values are presented in MPa



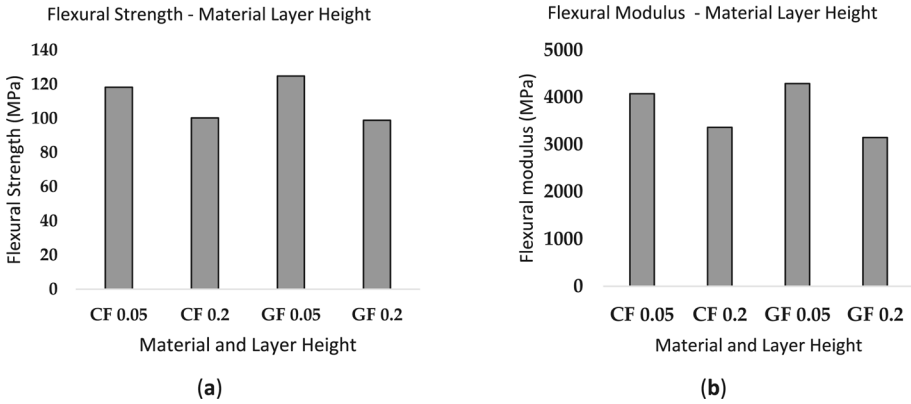


Fig. 12 Flexural strength and flexural modulus of the specimens; **a** flexural strength, **b** flexural modulus. All values are presented in MPa

accounts for interactions between phases and gives a value that often falls within the bounds set by Voigt and Reuss.

The Halpin-Tsai equations offer another means to estimate the effective moduli along the longitudinal ($E_{eff, long}$) and transverse ($E_{eff, trans}$) directions. For CFRP, these are 800 MPa and 371.4 MPa, and for GFRP, 1400 MPa and 371.4 MPa.

The experimental results show notable deviations. For CFRP with a layer height of 0.2 mm, the E_{eff} is 727.1 MPa, which is within the Voigt and Reuss and Halpin-Tsai bounds but deviates from the self-consistent model by 8.4%. For a layer height of 0.05 mm, CFRP has an E_{eff} of 652.4 MPa, which, too, is within the bounds of Voigt and Reuss and the Halpin-Tsai models but deviates from the self-consistent model approximately by 20.8%. GFRP, at a layer height of 0.2 mm, exhibits an E_{eff} of 842.5 MPa, which notably exceeds the theoretical prediction of the self-consistent model by 10.3%. For GFRP with 0.05 mm layer height, the experimental value is 1238.8 MPa, representing a significant deviation from the self-consistent model whilst remaining within the bounds of other models.

These incompatibilities between theoretical models and experimental data are likely due to the complexities introduced by the AM process, which alters the material properties of each phase considerably. The AM process further introduces cohesive regions between the layers, affecting the overall mechanical behaviour and deviating from the theoretically predicted values. Thus, while the models provide a reasonable first approximation, the intricacies of 3D-printed microstructures require more refined analytical or numerical models for precise prediction.

Table 5 Flexural strengths and Flexural moduli for 100% infill specimens

Group	CF 0.05	CF 0.2	GF 0.05	GF 0.2
Flexural Strength [MPa]	118.3	100.3	124.9	98.9
Young's Modulus (Flexural) [MPa]	4074.9	3362.0	4289.4	3145.4

All values are presented in MPa

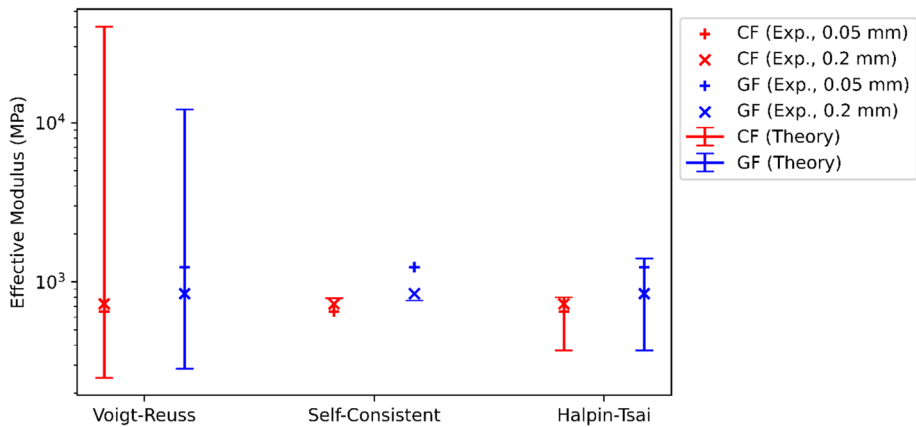


Fig. 13 Comparison of theoretical and experimental effective moduli for carbon and glass fibre reinforced polymers using various homogenisation techniques. All values are presented in MPa

6.4 Application of the Additively Manufactured Structures to Robotics

6.4.1 Topology Optimisation and Design of Drivetrain Skirts

TO plays a crucial role in refining the design of the drivetrain skirts. The first TO simulation demonstrates that material could be removed from the body of the skirt whilst retaining a central supportive structure. To avoid any impractical results, a 30% volume restriction is implemented when performing this TO. This also helps ensure that the skirt's aesthetic and protective functions are maintained, as shown in Fig. 14.

Based on these TO results, a final design is settled upon also considering manufacturability and printing requirements. It achieved a 30.3% weight reduction—from 441.5 grams to 307.7 grams—without compromising structural integrity. To check the final design, a static FEA of this adjusted design indicated a maximum deflection of 0.25 mm, which is deemed acceptable, as shown in Fig. 15.

Slicing parameters are fine-tuned in the 'Simplify3D' software to enhance printing efficiency. A cross-sectional view of the final optimised component is shown in Fig. 16. The red and green lines represent the outer shell, and the yellow lines represent the rectilinear infill pattern. Since the wall supports most of the load, it is critical to avoid voids in that region. The printer extrudes lines with a width of 0.6 mm which leads to a shell thickness of 1.2 mm on either side of the wall. With a total thickness of 3

Table 6 Comparison of theoretical and experimental effective moduli (E , in mpa) for carbon and glass fibre reinforced polymers using various homogenisation techniques

Material	Experimental	Voigt and Reuss	Self-Consistent	Halpin-Tsai
CF	$E_{CF\ 0.2}=727.1$	$E_{Voigt}=40160$	$E_{eff}=788.4$	$E_{eff,long}=800$
	$E_{CF\ 0.05}=652.4$	$E_{Reuss}=249.9$		$E_{eff,trans}=371.4$
GF	$E_{GF\ 0.2}=842.5$	$E_{Voigt}=12140$	$E_{eff}=763.5$	$E_{eff,long}=1400$
	$E_{GF\ 0.05}=1238.8$	$E_{Reuss}=285.1$		$E_{eff,trans}=371.4$

All values are presented in MPa

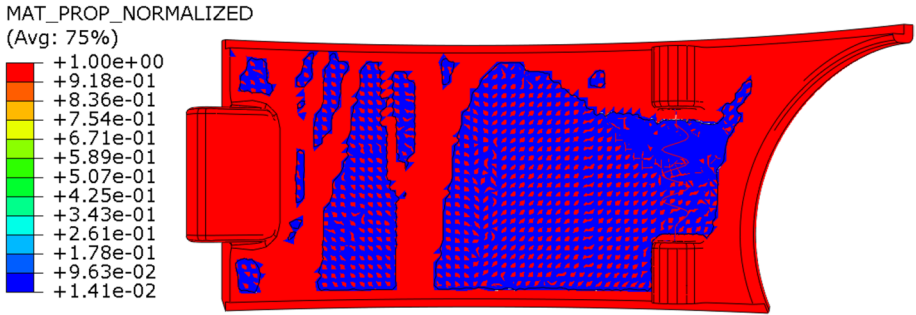


Fig. 14 Topology optimisation results for the drivetrain module skirt

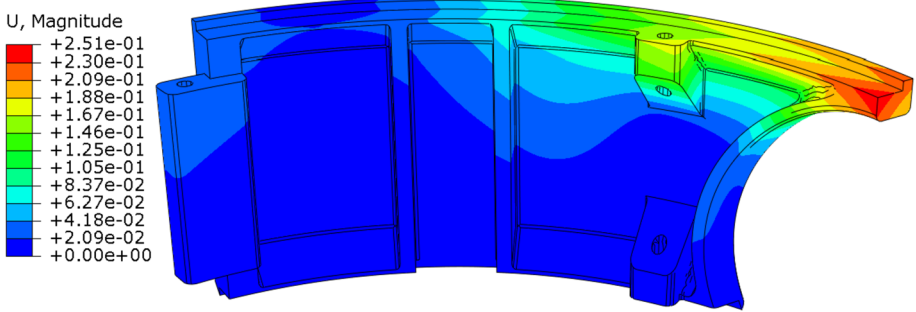


Fig. 15 FEA results for the final design of drivetrain module skirt. Deflections are presented in mm

mm, there is only 0.6 mm left in between the shells, which is just enough space for one solid line. These parameter choices facilitated a further reduction in weight without compromising the strength of the skirt. The benefits of topology and infill optimisation became evident when manufacturing the skirts, as the printing time is reduced to 19 hours from the original 30 hours, which also reduces energy and equipment costs. Since

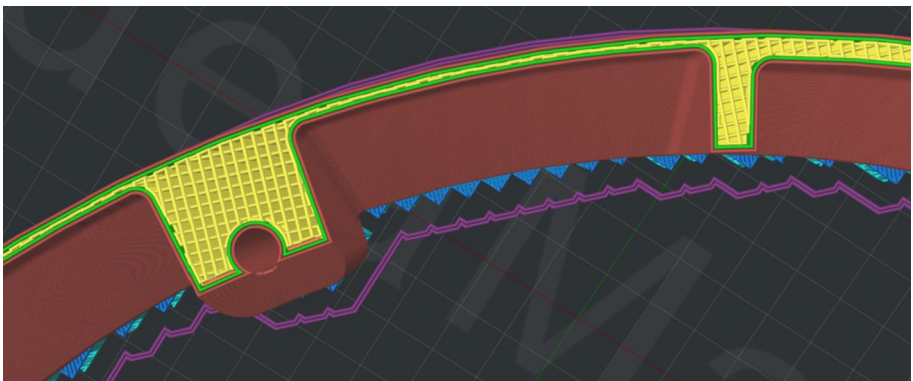


Fig. 16 Cross-sectional view of the final drivetrain module skirt in 'Simplify3D'

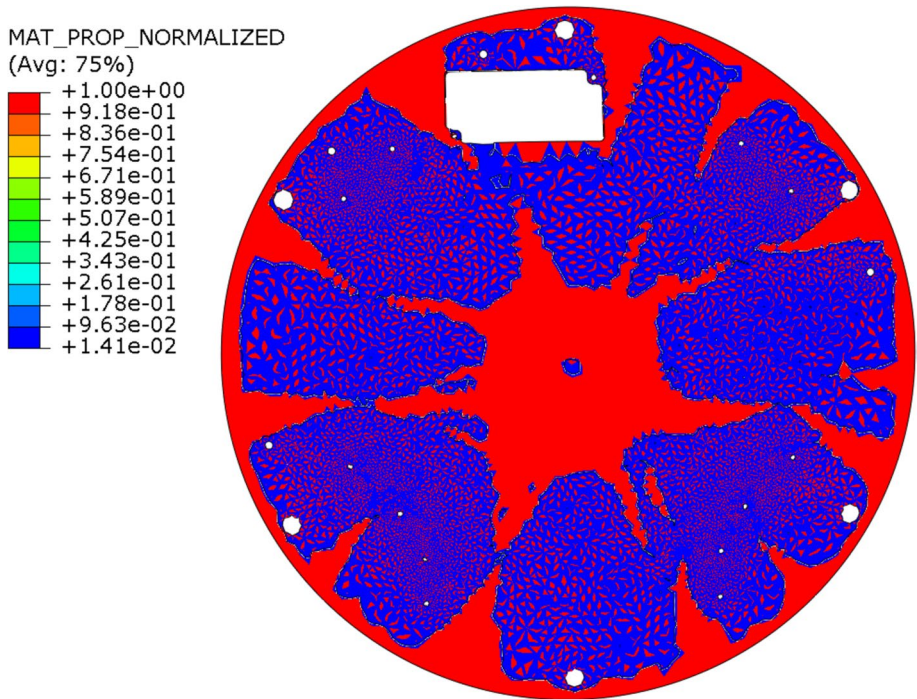


Fig. 17 Topology optimisation results for the support plate

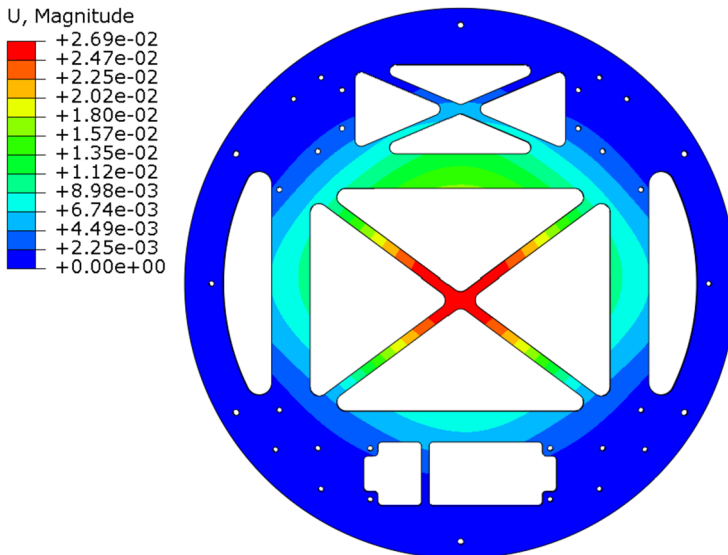


Fig. 18 FEA results for the final design of the support plate. Deflections are presented in mm

the filament cost is £0.08 per gram, the 133.8-gram weight reduction leads to a saving of £10.74; this is a significant value when considering mass production.

6.4.2 Topology Optimisation and Design of Support Plates

The TO results, as presented in Fig. 17, for the support plate inspire the design concept for the final design of the support plates. Although the exact 'star'-shaped pattern is not replicated, the core principle of distributing central loads to the plate's boundary is maintained. The final design leads to a 60% reduction in weight, from 1500 grams to 894 grams.

FEA estimated (Fig. 18) that the maximum deflection was well within acceptable limits, standing at 0.027 mm at the centre of the plate under realistic loading and boundary conditions.

7 Conclusions

This study systematically investigates the effects of infill densities and layer heights on the mechanical properties of GFRP and CFRP in (FDM) for robotic applications. The investigation is performed by employing a range of infill densities, namely 20%, 40%, 60%, and 100%, in tensile and three-point bending tests as well as microstructure visualisation through a microscope. This study reveals the changes in the strength and stiffness of 3D-printed composite structures. The results indicate a clear dependency on the infill density and layer height in strength and stiffness of 3D-printed composite structures pointing out the importance of the selection of the optimised printing parameters to achieve desired mechanical properties.

The experimental Young's moduli and tensile strength results are largely consistent with theoretical predictions, but there are some outliers. FDM prints are prone to defects that can cause a drastic change in mechanical properties. A statistical analysis with multiple copies of the same specimen would be the best method for quantifying the presence of defects.

Increasing infill density leads to elevated UTS, as expected. The trend is the same for Young modulus. The inconsistencies in the trend are judged to be caused by defects in printing processes. On the other hand, the effect of infill density is not highly significant, between 20% to 60%. The most effectiveness is obtained from 100% infill density.

Several theoretical approaches are utilised to predict these values, from classic homogenisation techniques like Voigt and Reuss bounds to more sophisticated models such as the self-consistent and Halpin-Tsai methods. These theoretical frameworks offer an efficient perspective on the prediction of mechanical properties of fibre-reinforced composites. Each comes with its own set of assumptions and limitations, thereby affecting its applicability and accuracy. A comparative assessment between these theoretical predictions and the experimental data is done. It must be noted that the experimental data generally resided within or proximate to the theoretically predicted bounds. However, this should not be perceived as a precise agreement between the theoretical models and experiments. The divergence between theory and experiment is not negligible. Even though, while theoretical models offer a range of possibilities for the effective modulus of composites, real-world processes like AM, introduce complexities that often result in values outside these bounds. Thereofre, this divergence is judged to be due to the complexities inherent in these

composite materials and structures, particularly when manufactured through AM methods. These deviations highlight the limitations of theoretical models in capturing the dominant interactions in composite materials.

The application of the additively manufactured composite structures is also performed in this study. The final geometries of the robotic components are designed employing topology optimisation, and they are additively manufactured. Not only did the final designs achieve significant weight and cost reductions, but they also meet structural integrity and operational requirements, thereby confirming the feasibility of using additively manufactured materials in robotic applications.

In the future, it would be interesting to conduct a statistical analysis with multiple specimens to gain more understanding of material flaws and their impacts on the static and fatigue characteristics. Using various polymer-fibre reinforcement combinations would also lay the groundwork for better tailorable materials and structures.

Acknowledgments The authors would like to thank UVRobots for their support to this research.

Author Contributions Arnav Bisoi: Methodology, Formal analysis, Investigation, Data curation, Writing-Original draft preparation.

Data Availability Statement All the data related to this research is present in the article.

Declarations

Conflicts of Interest The authors declare no conflict of interest. Mertol Tüfekci: Methodology, Formal analysis, Investigation, Data Curation, Writing- Reviewing and Editing. Vehbi Öztekin: Formal analysis, Investigation, Visualisation, Data Curation, Writing- Reviewing and Editing. Enora Denimal: Formal analysis, Investigation, Methodology, Writing- Reviewing and Editing, Supervision. Loïc Salles: Project Administration, Formal analysis, Methodology, Supervision.

Open Access This article is licensed under a Creative Commons Attribution 4.0 International License, which permits use, sharing, adaptation, distribution and reproduction in any medium or format, as long as you give appropriate credit to the original author(s) and the source, provide a link to the Creative Commons licence, and indicate if changes were made. The images or other third party material in this article are included in the article's Creative Commons licence, unless indicated otherwise in a credit line to the material. If material is not included in the article's Creative Commons licence and your intended use is not permitted by statutory regulation or exceeds the permitted use, you will need to obtain permission directly from the copyright holder. To view a copy of this licence, visit <http://creativecommons.org/licenses/by/4.0/>.

References

1. Dilberoglu, U.M., Gharehpapagh, B., Yaman, U., Dolen, M.: The role of additive manufacturing in the era of industry 4.0. *Procedia Manuf.* **11**, 545–554 (2017). <https://doi.org/10.1016/j.promfg.2017.07.148>
2. Lee, C.H., Padzil, F.N.B.M., Lee, S.H., Ainun, Z.M.A., Abdullah, L.C.: Potential for natural fiber reinforcement in pla polymer filaments for fused deposition modeling (Fdm) additive manufacturing: A review. *Polymers (Basel)* **13**, 1407 (2021). <https://doi.org/10.3390/polym13091407>
3. Marimuthu, S., Clark, D., Allen, J., Kamara, A.M., Mativenga, P., Li, L., Scudamore, R.: Finite element modelling of substrate thermal distortion in direct laser additive manufacture of an aero-engine component. *Proc. Inst. Mech. Eng. C J. Mech. Eng. Sci.* **227**, 1987–1999 (2013). <https://doi.org/10.1177/0954406212470363>
4. ASTM: Standard Terminology for Additive Manufacturing Technologies (2016)
5. Wang, X., Jiang, M., Zhou, Z., Gou, J., Hui, D.: 3D printing of polymer matrix composites: A review and prospective. *Compos. B Eng.* **110**, 442–458 (2017). <https://doi.org/10.1016/j.compositesb.2016.11.034>
6. Nath, S.D., Nilufar, S.: An overview of additive manufacturing of polymers and associated composites. *Polymers (Basel)* **12**, 1–33 (2020). <https://doi.org/10.3390/polym12112719>

7. Antony, S., Cherouat, A., Montay, G.: Fabrication and characterization of hemp fibre based 3D printed honeycomb sandwich structure by FDM process. *Appl. Compos. Mater.* **27**, 935–953 (2020). <https://doi.org/10.1007/s10443-020-09837-z>
8. Aw, Y.Y., Yeoh, C.K., Idris, M.A., Teh, P.L., Hamzah, K.A., Szali, S.A.: Effect of printing parameters on tensile, dynamic mechanical, and thermoelectric properties of FDM 3D printed CABS/ZnO composites. *Materials* **11** (2018). <https://doi.org/10.3390/ma11040466>
9. Suteja, T.J., Soesanti, A.: Mechanical Properties of 3D Printed Polylactic Acid Product for Various Infill Design Parameters: A Review. *J. Phys. Conf. Ser.* **1569** (2020). <https://doi.org/10.1088/1742-6596/1569/4/042010>
10. Khan, S.A., Siddiqui, B.A., Fahad, M., Khan, M.A.: Evaluation of the effect of infill pattern on mechanical strength of additively manufactured specimen. *Mater. Sci. Forum* **887** MSF, 128–132 (2017). <https://doi.org/10.4028/www.scientific.net/MSF.887.128>
11. Quill, T.J., Smith, M.K., Zhou, T., Baioumy, M.G.S., Berenguer, J.P., Cola, B.A., Kalaitzidou, K., Bougher, T.L.: Thermal and mechanical properties of 3D printed boron nitride – ABS composites. *Appl. Compos. Mater.* **25**, 1205–1217 (2018). <https://doi.org/10.1007/s10443-017-9661-1>
12. Chen, S., Li, D., Xiang, J., Zhao, S.: Composite manufacturing cost model targeting on design optimization. *Appl. Compos. Mater.* **27**, 673–691 (2020). <https://doi.org/10.1007/s10443-020-09828-0>
13. Wang, K., Xie, X., Wang, J., Zhao, A., Peng, Y., Rao, Y.: Effects of infill characteristics and strain rate on the deformation and failure properties of additively manufactured polyamide-based composite structures. *Results Phys.* **18**, (2020)
14. Kovan, V., Altan, G., Topal, E.S.: Effect of layer thickness and print orientation on strength of 3D printed and adhesively bonded single lap joints. *J. Mech. Sci. Technol.* **31**, 2197–2201 (2017). <https://doi.org/10.1007/s12206-017-0415-7>
15. Sood, A.K., Ohdar, R.K., Mahapatra, S.S.: Parametric appraisal of mechanical property of fused deposition modelling processed parts. *Mater. Des.* **31**, 287–295 (2010). <https://doi.org/10.1016/j.matdes.2009.06.016>
16. Gonabadi, H., Yadav, A., Bull, S.J.: The effect of processing parameters on the mechanical characteristics of PLA produced by a 3D FFF printer. *Int. J. Adv. Manuf. Technol.* **111**, 695–709 (2020). <https://doi.org/10.1007/s00170-020-06138-4>
17. Fernandez-Vicente, M., Calle, W., Ferrandiz, S., Conejero, A.: Effect of Infill Parameters on Tensile Mechanical Behavior in Desktop 3D Printing. *3D Print Addit Manuf.* **3**, 183–192 (2016). <https://doi.org/10.1089/3dp.2015.0036>
18. Ćwikła, G., Grabowik, C., Kalinowski, K., Paprocka, I., Ociepka, P.: The influence of printing parameters on selected mechanical properties of FDM/FFF 3D-printed parts. *IOP Conf. Ser. Mater. Sci. Eng.* **227**, (2017). <https://doi.org/10.1088/1757-899X/227/1/012033>
19. Sukindar, N.A. Bin, Bin, M.K.A.M.A., Hang Tuah Bin, B.T.B., Binti, C.N.A.J., Bin, M.I.S.I.: Analysis on the impact process parameters on tensile strength using 3d printer repetier-host software. *ARPN J. Engi. Appl. Sci.* **12**, 3341–3346 (2017)
20. Clausen, A., Aage, N., Sigmund, O.: Exploiting additive manufacturing infill in topology optimization for improved buckling load. *Engineering* **2**, 250–257 (2016). <https://doi.org/10.1016/J.ENG.2016.02.006>
21. Wu, J., Clausen, A., Sigmund, O.: Minimum compliance topology optimization of shell–infill composites for additive manufacturing. *Comput. Methods Appl. Mech. Eng.* **326**, 358–375 (2017). <https://doi.org/10.1016/j.cma.2017.08.018>
22. Cojocaru, V.: Influence of rectilinear infill parameters on mechanical behavior of 3D printed parts - a fem approach. *Robotica Manag.* **24**, 4–8 (2019)
23. Cojocaru, V., Miclosina, C.: Influence of rectilinear infill parameters on stress state of mechanical structures components. *Robotica Manag.* **25**, 4–12 (2020)
24. Plocher, J., Panesar, A.: Effect of density and unit cell size grading on the stiffness and energy absorption of short fibre-reinforced functionally graded lattice structures. *Addit Manuf.* **33**, (2020). <https://doi.org/10.1016/j.addma.2020.101171>
25. Peng, C., Fox, K., Qian, M., Nguyen-Xuan, H., Tran, P.: 3D printed sandwich beams with bioinspired cores: Mechanical performance and modelling. *Thin-Walled Struct.* **161**, (2021)
26. Becker, W.: Closed-form analysis of the thickness effect of regular honeycomb core material. *Compos. Struct.* **48**, 67–70 (2000). [https://doi.org/10.1016/S0263-8223\(99\)00074-4](https://doi.org/10.1016/S0263-8223(99)00074-4)
27. Nasirov, A., Fidan, I.: Prediction of mechanical properties of fused filament fabricated structures via asymptotic homogenization. *Mech. Mater.* **145** (2020). <https://doi.org/10.1016/j.mechmat.2020.103372>
28. Maskery, I., Ashcroft, I.A.: The deformation and elastic anisotropy of a new gyroid-based honeycomb made by laser sintering. *Addit Manuf.* **36**, (2020). <https://doi.org/10.1016/j.addma.2020.101548>

29. Zhang, H., Yang, D., Sheng, Y.: Performance-driven 3D printing of continuous curved carbon fibre reinforced polymer composites: A preliminary numerical study. *Compos. B Eng.* **151**, 256–264 (2018). <https://doi.org/10.1016/j.compositesb.2018.06.017>
30. Pascual-González, C., Iragi, M., Fernández, A., Fernández-Blázquez, J.P., Aretxabala, L., Lopes, C.S.: An approach to analyse the factors behind the micromechanical response of 3D-printed composites. *Compos. B Eng.* **186** (2020). <https://doi.org/10.1016/j.compositesb.2020.107820>
31. Yamawaki, M., Kouno, Y.: Fabrication and mechanical characterization of continuous carbon fiber-reinforced thermoplastic using a preform by three-dimensional printing and via hot-press molding. *Adv. Compos. Mater.* **27**, 209–219 (2018). <https://doi.org/10.1080/09243046.2017.1368840>
32. Abouzaid, K., Bassir, D., Guessasma, S., Yue, H.: Modelling the process of fused deposition modeling and the effect of temperature on the mechanical, roughness, and porosity properties of resulting composite products. *Mech. Compos. Mater.* **56**, 805–816 (2021). <https://doi.org/10.1007/s11029-021-09925-6>
33. Justo, J., Távora, L., García-Guzmán, L., París, F.: Characterization of 3D printed long fibre reinforced composites. *Compos. Struct.* **185**, 537–548 (2018). <https://doi.org/10.1016/j.compstruct.2017.11.052>
34. Kuncius, T., Rimašauskas, M., Rimašauskienė, R.: Interlayer adhesion analysis of 3d-printed continuous carbon fibre-reinforced composites. *Polymers (Basel)* **13** (2021). <https://doi.org/10.3390/polym13101653>
35. Hou, Z., Tian, X., Zhang, J., Li, D.: 3D printed continuous fibre reinforced composite corrugated structure. *Compos. Struct.* **184**, 1005–1010 (2018). <https://doi.org/10.1016/j.compstruct.2017.10.080>
36. Melenka, G.W., Cheung, B.K.O., Schofield, J.S., Dawson, M.R., Carey, J.P.: Evaluation and prediction of the tensile properties of continuous fiber-reinforced 3D printed structures. *Compos. Struct.* **153**, 866–875 (2016). <https://doi.org/10.1016/j.compstruct.2016.07.018>
37. Goh, G.D., Dikshit, V., An, J., Yeong, W.Y.: Process-structure-property of additively manufactured continuous carbon fiber reinforced thermoplastic: an investigation of mode I interlaminar fracture toughness. *Mech. Adv. Mater. Struct.* **0**, 1–13 (2020). <https://doi.org/10.1080/15376494.2020.1821266>
38. Bakis, C.E., Haluza, R.T., Bartolai, J., Kim, J.J., Simpson, T.W.: Assessment of anisotropic mechanical properties of a 3D printed carbon whisker reinforced composite. *Adv. Compos. Mater.* **28**, 545–560 (2019). <https://doi.org/10.1080/09243046.2019.1652030>
39. Balla, V.K., Kate, K.H., Satyavolu, J., Singh, P., Tadimeti, J.G.D.: Additive manufacturing of natural fiber reinforced polymer composites: Processing and prospects. *Compos. B Eng.* **174**, (2019)
40. Ivey, M., Melenka, G.W., Carey, J.P., Ayranci, C.: Characterizing short-fiber-reinforced composites produced using additive manufacturing. *Adv. Manuf. Polym. Compos. Sci.* **3**, 81–91 (2017). <https://doi.org/10.1080/20550340.2017.1341125>
41. Ning, F., Cong, W., Qiu, J., Wei, J., Wang, S.: Additive manufacturing of carbon fiber reinforced thermoplastic composites using fused deposition modeling. *Compos. B Eng.* **80**, 369–378 (2015). <https://doi.org/10.1016/j.compositesb.2015.06.013>
42. Nour, A., Mechakra, H., Benkoussas, B., Tawfiq, I., Settet, A.T., Renane, R.: Modeling a composite reinforced with short alfa fibers to determine its fatigue and structural homogenization. *Mech. Compos. Mater.* **54**, 487–498 (2018). <https://doi.org/10.1007/s11029-018-9758-0>
43. Nasirov, A., Gupta, A., Hasanov, S., Fidan, I.: Three-scale asymptotic homogenization of short fiber reinforced additively manufactured polymer composites. *Compos. B Eng.* **202**, (2020). <https://doi.org/10.1016/j.compositesb.2020.108269>
44. Al Abadi, H., Thai, H.T., Paton-Cole, V., Patel, V.I.: Elastic properties of 3D printed fibre-reinforced structures. *Compos. Struct.* **193**, 8–18 (2018). <https://doi.org/10.1016/j.compstruct.2018.03.051>
45. Tüfekci, M., Özkal, B., Maharaj, C., Liu, H., Dear, J.P., Salles, L.: Strain-rate-dependent mechanics and impact performance of epoxy-based nanocomposites. *Compos. Sci. Technol.* **233**, (2023)
46. Tekinalp, H.L., Kunc, V., Velez-Garcia, G.M., Duty, C.E., Love, L.J., Naskar, A.K., Blue, C.A., Ozcan, S.: Highly oriented carbon fiber-polymer composites via additive manufacturing. *Compos. Sci. Technol.* **105**, 144–150 (2014). <https://doi.org/10.1016/j.compscitech.2014.10.009>
47. Griffini, G., Invernizzi, M., Levi, M., Natale, G., Postiglione, G., Turri, S.: 3D-printable CFR polymer composites with dual-cure sequential IPNs. *Polymer (Guildf)* **91**, 174–179 (2016). <https://doi.org/10.1016/j.polymer.2016.03.048>
48. Naima Khalid, N., Afiqah Mohd Radzuan, N., Bakar Sulong, A., Mohd Foudzi, F.: A review on bonding of Polyamide reinforced carbon fibre via additive manufacturing. *IOP Conf. Ser. Mater. Sci. Eng.* **1078**, 012004 (2021). <https://doi.org/10.1088/1757-899x/1078/1/012004>
49. Abderrafai, Y., Hadi Mahdavi, M., Sosa-Rey, F., Hérard, C., Otero Navas, I., Piccirelli, N., Lévesque, M., Thériault, D.: Additive manufacturing of short carbon fiber-reinforced polyamide composites by fused filament fabrication: Formulation, manufacturing and characterization. *Mater. Des.* **214**, (2022)

50. Al Rashid, A., Ikram, H., Koç, M.: Additive manufacturing and mechanical performance of carbon fiber reinforced Polyamide-6 composites. *Mater. Today Proc.* **62**, 6359–6363 (2022). <https://doi.org/10.1016/j.matpr.2022.03.339>
51. K., P., M., M., P., S.P.: Technologies in additive manufacturing for fiber reinforced composite materials: a review. *Curr. Opin. Chem. Eng.* **28**, 51–59 (2020). <https://doi.org/10.1016/j.coche.2020.01.001>
52. Jansson, A., Pejryd, L.: Characterisation of carbon fibre-reinforced polyamide manufactured by selective laser sintering. *Addit. Manuf.* **9**, 7–13 (2016). <https://doi.org/10.1016/j.addma.2015.12.003>
53. Roy, R., Park, S.J., Kweon, J.H., Choi, J.H.: Characterization of Nomex honeycomb core constituent material mechanical properties. *Compos. Struct.* **117**, 255–266 (2014). <https://doi.org/10.1016/j.compstruct.2014.06.033>
54. Li, N., Link, G., Wang, T., Ramopoulos, V., Neumaier, D., Hofele, J., Walter, M., Jelonnek, J.: Path-designed 3D printing for topological optimized continuous carbon fibre reinforced composite structures. *Compos. B Eng.* **182**, (2020)
55. Srivastava, M., Rathee, S.: Optimisation of FDM process parameters by Taguchi method for imparting customised properties to components. *Virtual Phys. Prototyp.* **13**, 203–210 (2018). <https://doi.org/10.1080/17452759.2018.1440722>
56. Zhang, Y., Chou, Y.K.: Three-dimensional finite element analysis simulations of the fused deposition modelling process. *Proc. Inst. Mech. Eng. B J. Eng. Manuf.* **220**, 1663–1671 (2006). <https://doi.org/10.1243/09544054JEM572>
57. Bellehumeur, C., Li, L., Sun, Q., Gu, P.: Modeling of bond formation between polymer filaments in the fused deposition modeling process. *J. Manuf. Proc.* **6**, 170–178 (2004). [https://doi.org/10.1016/S1526-6125\(04\)70071-7](https://doi.org/10.1016/S1526-6125(04)70071-7)
58. Penumakala, P.K., Santo, J., Thomas, A.: A critical review on the fused deposition modeling of thermoplastic polymer composites. *Compos. B Eng.* **201**, (2020)
59. Lieneke, T., Denzer, V., Adam, G.A.O., Zimmer, D.: Dimensional tolerances for additive manufacturing: Experimental investigation for fused deposition modeling. *Procedia CIRP* **43**, 286–291 (2016). <https://doi.org/10.1016/j.procir.2016.02.361>
60. Wittbrodt, B., Pearce, J.M.: The effects of PLA color on material properties of 3-D printed components. *Addit. Manuf.* **8**, 110–116 (2015). <https://doi.org/10.1016/j.addma.2015.09.006>
61. Ziemian, C., Sharma, M., Ziem, S.: Anisotropic mechanical properties of ABS parts fabricated by fused deposition modelling. *Mech. Eng.* (2012). <https://doi.org/10.5772/34233>
62. Alaimo, G., Marconi, S., Costato, L., Auricchio, F.: Influence of meso-structure and chemical composition on FDM 3D-printed parts. *Compos. B Eng.* **113**, 371–380 (2017). <https://doi.org/10.1016/j.compositesb.2017.01.019>
63. Romanowski, H., Bierkandt, F.S., Luch, A., Laux, P.: Summary and derived risk assessment of 3D printing emission studies. *Atmos. Environ.* **294**, (2023)
64. Parandoush, P., Lin, D.: A review on additive manufacturing of polymer-fiber composites. *Compos. Struct.* **182**, 36–53 (2017). <https://doi.org/10.1016/j.compstruct.2017.08.088>
65. Vaezi, M., Yang, S.: Extrusion-based additive manufacturing of PEEK for biomedical applications. *Virtual Phys. Prototyp.* **10**, 123–135 (2015). <https://doi.org/10.1080/17452759.2015.1097053>
66. Denimal, E., El Haddad, F., Wong, C., Salles, L.: Topological optimization of under-platform dampers with moving morphable components and global optimization algorithm for nonlinear frequency response. *Proc. ASME Turbo Expo. 2D-2020* (2020). <https://doi.org/10.1115/GT2020-14394>
67. ASTM-D882-10: Standard Test Method for Tensile Properties of Plastics. (2010)
68. ASTM INTERNATIONAL: Standard Test Methods for Flexural Properties of Unreinforced and Reinforced Plastics and Electrical Insulating Materials. D790. Annual Book of ASTM Standards. 1–12 (2002). <https://doi.org/10.1520/D0790-17.2>
69. Baich, L., Manogharan, G., Marie, H.: Study of infill print design on production cost-time of 3D printed ABS parts. *Int. J. Rapid Manuf.* **5**, 308–319 (2015)
70. Materials, P., Materials, E.I., Matrix, P., Materials, C., Specimens, P.: Standard Test Method for Tensile Properties of Plastics. **1**, 1–15 (2006). <https://doi.org/10.1520/D0638-14.1>
71. Barbero, E.J.: Finite element analysis of composite materials using Abaqus. (2013)
72. Gay, D., Hoa, S. V., Tsai, S.W.: Composite materials: Design and applications. (2002)
73. Ngo, T.D., Kashani, A., Imbalzano, G., Nguyen, K.T.Q., Hui, D.: Additive manufacturing (3D printing): A review of materials, methods, applications and challenges. *Compos. B Eng.* **143**, 172–196 (2018). <https://doi.org/10.1016/j.compositesb.2018.02.012>
74. Omar, N.W.Y., Shuaib, N.A., Hadi, M.H.J.A., Azmi, A.I.: Mechanical properties of carbon and glass fibre reinforced composites produced by additive manufacturing: A short review. *IOP Conf. Ser. Mater. Sci. Eng.* **670** (2019). <https://doi.org/10.1088/1757-899X/670/1/012020>

75. Tüfekci, M.: Performance evaluation analysis of Ti-6Al-4V foam fan blades in aircraft engines: A numerical study. *Compos. Part C: Open Access* **12**,(2023)
76. Fuller, J., Mitchell, S., Pozegic, T., Wu, X., Longana, M., Wisnom, M.: Experimental evaluation of hygro-thermal effects on pseudo-ductile thin ply angle-ply carbon/epoxy laminates. *Compos. B Eng.* **227**,(2021)
77. Acarer, S., Pir, İ., Tüfekci, M., Erkoç, T., Güneş Durak, S., Öztekin, V., Türkoğlu Demirkol, G., Özçoban, M.Ş., Temelli Çoban, T.Y., Çavuş, S., Tüfekci, N.: Halloysite nanotube-enhanced polyacrylonitrile ultra-filtration membranes: Fabrication, characterization, and performance evaluation. *ACS Omega* **8**, 34729–34745 (2023). <https://doi.org/10.1021/acsomega.3c03655>
78. Acarer, S., Pir, İ., Tüfekci, M., Erkoç, T., Öztekin, V., Durak, S.G., Özçoban, M.Ş., Demirkol, G.T., Alhammod, M., avuş, S., Tüfekci, N.: Characterisation and modelling the mechanics of cellulose nanofibril added polyethersulfone ultrafiltration membranes. *Heliyon* **9**, e13086 (2023). <https://doi.org/10.1016/j.heliyon.2023.e13086>
79. Acarer, S., Pir, İ., Tüfekci, M., Erkoç, T., Öztekin, V., Dikicioğlu, C., Demirkol, G.T., Durak, S.G., Özçoban, M.Ş., Çoban, T.Y.T., Çavuş, S., Tüfekci, N.: Characterisation and Mechanical Modelling of Polyacrylonitrile-Based Nanocomposite Membranes Reinforced with Silica Nanoparticles. *Nanomaterials* **12**, 3721 (2022). <https://doi.org/10.3390/nano12213721>

Publisher's Note Springer Nature remains neutral with regard to jurisdictional claims in published maps and institutional affiliations.